Pergamon

Tetrahedron 57 (2001) 7883–7892

TETRAHEDRON

Electronic absorption spectra of closed and open-shell tetrathiafulvalenes: the first time-dependent density-functional study

Raquel Andreu, Javier Garín and Jesús Orduna*

Departamento de Química Orgánica, ICMA, Universidad de Zaragoza-CSIC, E-50009 Zaragoza, Spain

Received 5 April 2001; revised 2 July 2001; accepted 25 July 2001

Abstract—The lowest energy transitions of tetrathiafulvalene (TTF) derivatives are calculated at different levels of theory. Whereas semiempirical (CNDO/S, ZINDO) and HF methods (CIS, TD-HF) give unrealistic excitation energies, time-dependent density-functional theory (TD-DFT) calculations provide a much improved description of the electronic absorption spectra of these compounds, including the unusual behavior of some TTF-containing nonlinear optical chromophores. Moreover, the study of radical cations of TTF derivatives allows the evaluation of the performance of TD-DFT methods on sulfur-containing open-shell species for the first time.

1. Introduction

Interest in tetrathiafulvalene (TTF) chemistry[1] has spanned the last thirty years, since the electron-donor properties of TTF derivatives have led to a wealth of organic conductors and superconductors.[2] Moreover, it has recently been recognized that the extraordinary electronic properties of TTF could be used in the development of redox-switchable complexating crown ethers,[3] electroactive Langmuir–Blodgett films,[4] building blocks in supramolecular chemistry,[5] and donor–σ-acceptor compounds showing intramolecular charge-transfer properties,[6] such as TTF–σ-C_{60} derivatives, which show efficient charge separation in the excited state[7] and are promising materials for artificial photosynthetic systems and molecular electronic devices.[8]

In a similar vein, we have recently demonstrated that TTF–π-acceptor molecules are efficient second-order nonlinear optical (NLO) chromophores,[9] which show a rather unusual optical behavior: the expected increase in their $\mu\beta_0$ values on lengthening the π-spacer is accompanied by a hypsochromic shift of their maximum wavelength absorption bands. This effect constitutes a notorious exception to the well-known transparency-nonlinear efficiency trade-off[10] and, therefore, it can be exploited in the search of more efficient and more transparent second-order NLO chromophores.

To allow a rational design of these kind of compounds, a reliable prediction of their absorption spectra is mandatory. To that end, both semiempirical and Hartree–Fock methods have been widely used. Moreover, the recent advent of time-dependent density functional theory (TD-DFT) methods[11] has led in many cases to the calculation of the optical properties of organic (and metallo-organic) species with a similar accuracy to that of more sophisticated CASSCF methods and at lower computational cost. On the other hand, very few organic sulfur compounds have been studied by TD-DFT methods[12] and, to the best of our knowledge, their performance with TTF derivatives has not been tested yet.

In this work, we have studied the performance of different quantum chemical calculations for predicting the electronic absorption spectra of TTF and $TTF^{+\cdot}$, by comparing their results to experimental data. TD-DFT methods, giving the most satisfactory results in this benchmark study, have been applied to other neutral and charged TTF derivatives. The results of these calculations allow a rationale for the interpretation of: (a) the widely different (and disputed) optical properties displayed by TTF radical cation salts bearing peripheral chalcogen atoms or not and (b) the remarkable hypsochromic effect displayed by some TTF–π-acceptor chromophores on lengthening the polyenic π-spacer.

2. Results and discussion

2.1. The UV–vis spectrum of TTF

2.1.1. Experimental data and previous interpretations. Although the UV–vis spectrum of TTF (**1**, Fig. 1) in several

Keywords: electronic spectra; thiafulvalenes; theoretical studies.
* Corresponding author. Fax: +34-976-761194;
e-mail: jorduna@posta.unizar.es

0040–4020/01/$ - see front matter
PII: S0040-4020(01)00766-9

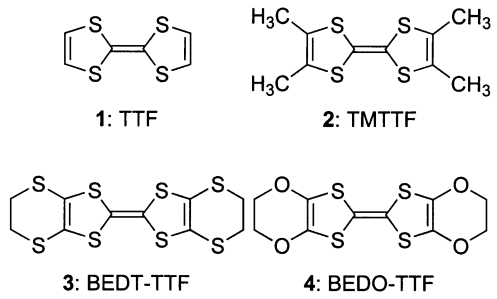

Figure 1. Structures of studied TTF derivatives.

solvents has been reported,[13] we will pay attention to the spectra recorded in non polar solvents such as hexane[14] or cyclohexane.[15] The spectrum recorded under these conditions shows four absorption bands above 300 nm: a very weak (ϵ=270) absorption at 450 nm (2.76 eV), a weak absorption (ϵ=1900) at 368 nm (3.37 eV) and two intense bands (ϵ=21500 and ϵ=13000) at 317 and 303 nm (3.91 and 4.09 eV, respectively). The polarized-light spectrum of the three lowest energy absorption bands has also been reported[16] and indicates that the band at 2.76 eV is polarized both in the long and the short axes of the molecule. The band at 3.37 eV is polarized along the short axis and the only band described at about 4.0 eV is polarized in the long axis. The double polarization of the lowest energy absorption was explained[17] on the basis of either two superposed forbidden transitions or a transition displaying a polarization perpendicular to the molecular plane that appears to have double polarization due to slightly misaligned molecules.[18]

Attempts to assign these transitions have made use of different theoretical methods, such as PPP,[19] extended Hückel,[15] MINDO/3[20] and more recently CNDO/S,[21] which also lead to different conclusions. Thus, PPP predicts quite accurately the energy of the transitions at 3.37 and 4.09 eV but does not reproduce the lowest energy absorption band which is attributed to a $n\rightarrow\pi^*$[19] or to a forbidden $\pi\rightarrow\pi^*$[16] transition; extended Hückel calculations[15] assign the bands at 2.76 and 3.37 eV as a $\pi\rightarrow\sigma^*$ transitions and the 3.91 eV band as $\pi\rightarrow\pi^*$; MINDO/3 predicts[20] $\pi\rightarrow\pi^*$ transitions for the absorptions at 3.37 and 3.91 eV and suggests that σ orbitals are involved in the lowest energy band. The configuration interaction and the spectroscopy optimized CNDO/S[21] analysis concludes that the 2.76 eV band corresponds to a HOMO→LUMO transition with $\pi\rightarrow\sigma^*$ character, and the bands at 3.91 and 4.09 eV are two nearly degenerated $\pi\rightarrow\pi^*$ transitions; an assignment for the absorption at 3.17 eV is lacking and finally, a Hartree–Fock–Slater calculation[18] predicts the correct polarization of the three lowest energy absorptions but a prediction of the energy of these transitions is not given.

2.1.2. Calculations. Considering that none of the methods reported up to date describes unambiguously the UV–vis spectrum of TTF we were prompted to the search for a theoretical method providing a precise qualitative and quantitative description and thus, we have performed calculations increasing the complexity and computational cost from semiempirical to ab initio Hartree–Fock based calculations and finally DFT methods.

In order to perform semiempirical calculations, TTF was optimized within the D_{2h} symmetry using the PM3[22] Hamiltonian and electronic excitations were calculated using CNDO/S[23] and ZINDO[24] methods. According to these calculations, the three lowest energy transitions are due to one $\pi\rightarrow\sigma^*$ and two $\pi\rightarrow\pi^*$ transitions but the calculated energies, ranging from 5.4 to 6.9 eV (CNDO/S) or from 5.2 to 6.8 eV (ZINDO), are far above the experimental values and indicate that the parameterization of these methods is not adequate for TTF.

Ab initio Hartree–Fock based calculations led to results that were similar to those of semiempirical methods; thus the CIS[25]/6-31G*//HF/6-31G* model chemistry predicted a weak HOMO→LUMO band due to a $\pi\rightarrow\sigma^*$ transition at 4.00 eV and two intense bands corresponding to $\pi\rightarrow\pi^*$ transitions at 6.00 and 6.12 eV while the TD-HF[26] method using the same geometry and basis set led to analogous predictions with somewhat lower excitation energies (3.96, 5.75 and 5.94 eV, respectively). The use of the 6-31+G* basis set incorporating diffuse functions on heavy atoms resulted in minor changes in the predicted energies. The results of semiempirical and Hartree–Fock based calculations are gathered in Table 1.

Table 1. Computed energies (eV) (λ (nm)=1239.84/E (eV)) with parenthesized oscillator strengths ($10^4 f$) for the lowest energy electronic excitations of TTF (**1**) calculated by non-DFT methods

Method	Transition[a]			
	B_{3u}	B_{1u}	B_{2u}	B_{1u}
Experimental[b]	2.76 (270)	3.37 (1900)	3.91 (2150)	4.09 (13000)
CNDO/S[c]	5.43 (4336)	6.07 (667)	5.70 (2251)	6.93 (2304)
ZINDO[c]	5.18 (3848)	5.40 (668)	5.25 (1932)	6.84 (1442)
CIS/6-31G*[d]	4.00 (2)	6.00 (7670)	6.12 (2691)	–
CIS/6-31+G*[d]	3.95 (7)	5.63 (6226)	5.63 (2511)	–
TD-HF/6-31G*[d]	3.96 (2)	5.75 (6233)	5.94 (2190)	–
TD-HF/6-31+G*[d]	3.91 (8)	5.44 (5375)	5.49 (2047)	–

Transitions are assigned according to their polarization.
[a] The TTF molecule is placed at the standard orientation of a D_{2h} point group: the z axis corresponds to the long molecular axis, y to the short axis and x is perpendicular to the molecular plane.
[b] Energies (eV) with parenthesized ϵ values, Ref. 15.
[c] PM3 optimized geometry.
[d] HF/6-31G* optimized geometry.

Table 2. Computed energies (eV) with parenthesized oscillator strengths (10^4 *f*) for the lowest energy electronic excitations of TTF (**1**) calculated by TD-DFT methods

		Transition[a]				
Functional	Basis set	A_1 52→53	B_1 52→54	A_2 52→55	B_2 52→58	B_1 52→57
B3LYP	6-31G*	2.64 (1)	3.57 (132)	4.03 (0)	3.97 (101)	4.06 (269)
	6-31+G*	2.63 (2)	3.40 (181)	3.87 (0)	3.80 (164)	3.86 (264)
	6-311+G**	2.67 (2)	3.36 (204)	3.82 (0)	3.85 (194)	3.84 (215)
	cc-PVDZ	2.73 (1)	3.51 (192)	3.89 (0)	4.10 (130)	4.07 (142)
	aug-cc-PVDZ	2.69 (2)	3.29 (197)	–	3.83 (226)	3.83 (131)
B3P86	6-31G*	2.69 (1)	3.51 (142)	4.00 (0)	4.07 (233)	4.18 (271)
	6-31+G*	2.68 (1)	3.37 (181)	3.88 (0)	3.96 (359)	4.03 (269)
	6-311+G**	2.72 (1)	3.33 (199)	3.82 (0)	4.02 (471)	4.01 (232)
	cc-PVDZ	2.77 (1)	3.44 (176)	3.88 (0)	4.19 (345)	4.20 (164)
	aug-cc-PVDZ	2.74 (2)	3.25 (177)	3.79 (0)	4.01 (599)	4.00 (154)
B3PW91	6-31G*	2.69 (1)	3.52(147)	4.00 (0)	4.06 (221)	4.16 (266)
	6-31+G*	2.68 (1)	3.38 (184)	3.87 (0)	3.94 (343)	4.00 (263)
	6-311+G**	2.72 (1)	3.33 (200)	3.82 (0)	3.99 (435)	3.99 (226)
	cc-PVDZ	2.77 (1)	3.44 (180)	3.88 (0)	4.18 (323)	4.19 (160)
	aug-cc-PVDZ	2.74 (2)	3.25 (180)	3.78 (0)	3.97 (561)	3.97 (150)
Experimental (cyclohexane)[b]		2.76 (270)	3.37 (1900)	–	3.91 (21500)	4.09 (13000)

Transitions are assigned according to their polarization.
[a] The TTF molecule is placed at the standard orientation of a C_{2v} point group as depicted in Fig. 2.
[b] Energies (eV) with parenthesized ϵ values, Ref. 15.

The large errors obtained using the above mentioned methods prompted us to use TD-DFT calculations, since these methods are reported to afford excitation energies which are in good agreement with experimental ones.[11] Within this approach, hybrid functionals are usually superior to conventional ones[11a,27] and although B3LYP[28] is the most widely used hybrid functional, it has been reported that B3P86[29] and B3PW91[30] appear to be somewhat better at reproducing the observed transition energies.[31] Therefore, we decided to test the reliability of these three functionals on TTF. The geometry of TTF was optimized using the 6-31G* basis set and the corresponding functional. As previously reported,[32] the geometry optimization of TTF by DFT leads to a boat-like shape with C_{2v} symmetry. The B3LYP optimization of TTF[33] gives C–S bond lengths that are too long in agreement with previous studies on compounds with third row elements.[34] On the other hand, the B3P86 functional, which yields better sulfur bond lengths,[35] reproduces[32a,36] accurately, the gas phase electron diffraction structure of TTF.[37] The B3PW91 optimized geometry is nearly identical to that obtained using the B3P86 functional.

Single point TD-DFT calculations were performed using the following basis sets: 6-31G*[38], 6-31+G*, 6-311+G**[39] and the correlation consistent basis sets[40] with (aug-CC-PVDZ) or without (CC-PVDZ) diffuse functions. The results of these calculations are gathered in Table 2. It can be seen that there is an excellent agreement between the calculated and the theoretical values and that the choice of the functional and basis set plays little influence on the calculation results. Estimation of the root mean square errors and maximum absolute deviations reveals that the B3P86/6-31+G* model chemistry gives rise to the more accurate results with absolute deviations of less than 0.1 eV but even the medium size 6-31G* basis set gives rise to accurate results at a lower computational cost.

According to these TD-DFT calculations, the molecular orbitals are those depicted in Fig. 2. The lowest energy absorption band corresponds to a $\pi\rightarrow\sigma^*$ transition from the HOMO (MO52, symmetry a_1) to the LUMO (MO53, symmetry a_1) and consequently is an A_1 transition displaying *z* polarization. The second transition occurring at 3.37 eV is an excitation from the HOMO to the LUMO+1 (MO54, b_1) and thus corresponds to a $\pi\rightarrow\pi^*$ transition with

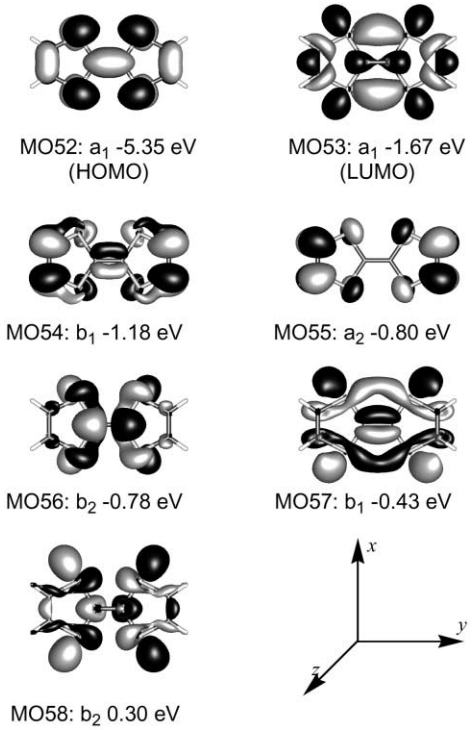

Figure 2. Molecular orbitals of TTF: B3P86/6-31+G*//B3P86/6-31G* (C_{2v}).

B_1 symmetry and x polarization. The excitation from the HOMO to the LUMO+2 (MO55, a_2) is calculated at about 3.9 eV but is an A_2 symmetry forbidden transition and the two most intense bands in the spectrum correspond to excitations from the HOMO to MO58 (B_2, y polarized) and MO57 (B_1, x polarized).

To sum up, TD-DFT calculations match precisely the absorption energies, the calculated oscillator strengths reproduce the relative intensity of the bands and the calculated polarizations are also in good agreement with the experiment.

2.2. The UV–vis spectra of TTF derivatives

In order to explore the scope of these calculations we have also studied TTF derivatives **2**–**4** (Fig. 1) using the model chemistry that yields the best results with TTF (B3P86/6-31+G*//B3P86/6-31G*). The first studied derivative was tetramethyltetrathiafulvalene **2** (TMTTF) since the polarized spectrum of this compound in a stretched polyethylene film has been described[20] and the calculated polarization can thus be compared with the experiment. The electronic transitions calculated for TMTTF are analogous to that of TTF and are in good agreement with the experimental data obtained in 1,2-dichloroethane solution (Table 3).[14b] Furthermore, the calculated polarizations in the short axis for the transitions at 3.63 and 4.25 eV and in the long axis for the band at 3.74 eV are in good agreement with the experimental polarizations observed in the polyethylene film.

Geometry optimization on bis(ethylenedithio)tetrathiafulvalene **3** (BEDT-TTF) and bis(ethylenedioxy)tetrathiafulvalene **4** (BEDO-TTF) located a minimum of C_2 symmetry in agreement with previously reported[33,41] calculations performed on BEDT-TTF and with the reported X-ray structures of BEDT-TTF[42] and BEDO-TTF.[43] Furthermore, the rms error when comparing the calculated bond lengths to those measured in their X-ray structures is only 0.006 Å for BEDT-TTF and 0.014 Å for BEDO-TTF.

The TD-DFT method applied to BEDT-TTF (Table 3) predicts five allowed transitions below 4.0 eV that are in good correspondence with the five lowest energy transitions calculated for TTF. The first two transitions calculated at 2.75 and 3.46 eV are in close agreement with the experimental 2.66 and 3.55 eV bands obtained in 1,1,2-trichloroethane solution.[44] The third one calculated at 3.76 eV corresponds to a forbidden transition in TTF that becomes allowed due to the lower symmetry of BEDT-TTF. Similar energy calculated for three of the transitions (3.62, 3.76, 3.84 eV) may be responsible for their appearance as a single intense band at 3.83 eV in the experimental spectrum.

The calculated excitation energies and oscillator strengths of BEDO-TTF (Table 3) are also in sharp correspondence with the reported absorptions in acetonitrile solution.[43,45] Moreover, we have recorded the UV–vis spectrum of **4** in the same solvent and a closer inspection discloses a previously unreported shoulder[46] at ca. 3.35 eV which agrees extremely well with the predicted absorption at 3.28 eV. On the other hand, the calculated transition at 3.74 eV may well be hidden by the intense band observed at 3.68 eV.

2.3. UV–vis spectra of radical cations of TTF derivatives

2.3.1. $TTF^{+\cdot}$. The UV–vis spectra of $TTF^{+\cdot}$ recorded using different solvents[13b–f,15,47] display some common features: The lowest energy absorption band is observed at ca. 580 nm (2.14 eV), the most intense band is located at ca. 435 nm (2.85 eV) and two weak bands are visible depending on the experimental conditions at about 2.52 and 3.08 eV. The polarized absorption spectra of single crystals of $(TTF)(ClO_4)$ have also been reported,[48] and indicate that the two intense absorptions (2.14 and 2.85 eV) are polarized in the b axis of the crystal, which according to its structure[49] corresponds to the long axis of the molecule, while the weak absorptions show polarization in the a axis and, considering the arrangement of molecules in the crystal, it can be due to absorptions polarized either in the short axis of the $TTF^{+\cdot}$ or in an axis perpendicular to the molecular plane. In a similar way, the polarized light spectra of radical salts of BEDT-TTF[50] and similar derivatives[51] suggest that the intense absorption bands are polarized in the long axis of the TTF radical ions although the molecular axes are not perfectly aligned with the crystallographic axes.

Previous attempts made in order to explain the absorption spectrum of $TTF^{+\cdot}$ involved the use of semiempirical calculations. The first of them,[19] that made use of PPP, provided a

Table 3. Calculated (TD-B3P86/6-31+G*//B3P86/6-31G*) and experimental lowest energy transitions of TTF derivatives. Transitions involving analogous orbitals are arranged within the same row of the table

	TMTTF (**2**)				BEDT-TTF (**3**)				BEDO-TTF (**4**)			
	Calcd		Exp.[a]		Calcd		Exp.[b]		Calcd		Exp.[c]	
Symmetry[d]	E (eV)	$10^4\ \pi$	E (eV)	Log ϵ	E (eV)	$10^4\pi$	E (eV)	Log ϵ	E (eV)	$10^4\pi$	E (eV)	Log ϵ
A	2.61	4	2.62	2.4	2.75	0	2.66	2.4	2.40	0	2.40	2.2
B	3.63	342	3.79	4.1	3.46	342	3.55	4.0	3.82	170	3.68	4.0
A	4.12	0	–	–	3.76	1	–	–	–	–	–	–
B	3.74	488	3.94	4.1	3.62	881	3.83	4.2	4.10	3319	3.94	4.1
B	4.25	511	4.32	4.1	3.84	364	–	–	3.28	1	–	–
B	–	–	–	–	–	–	–	–	3.74	15	–	–

[a] In 1,2-dichloroethane, Ref. 14b.
[b] In 1,1,2-trichloroethane, Ref. 44.
[c] In acetonitrile, Ref. 43.
[d] The standard orientation was used, the z axis corresponding to the C_2 axis.

Table 4. Computed energies (eV) with parenthesized oscillator strengths (10^4 *f*) for the lowest energy electronic excitations of $TTF^{+\cdot}$ ($\mathbf{1}^{+\cdot}$) calculated by different methods

		Transition[a]			
Method	Basis set	B_{1u}	B_{3u}	B_{1u}	B_{2u}
ZINDO[b]	–	1.81 (2087)	–	2.83 (1299)	2.27 (11)
CIS[c]	6-31G*	2.85 (1651)	4.16 (1)	3.80 (3091)	3.88 (62)
	6-31+G*	2.84 (1630)	4.14 (1)	3.75 (3085)	3.86 (61)
TD-HF[c]	6-31G*	2.31 (2344)	4.09 (1)	3.32 (2224)	2.03 (151)
	6-31+G*	2.30 (2341)	4.07 (2)	3.28 (2219)	2.09 (156)
TD-B3P86[d]	6-31G*	2.37 (738)	2.69 (1)	3.43 (3049)	3.37 (38)
	6-31+G*	2.35 (735)	2.68 (1)	3.39 (3075)	3.30 (47)
	6-31G(2d,p)	2.34 (620)	2.57 (1)	3.33 (2950)	3.20 (50)
	6-311G(2d,p)	2.35 (568)	2.58 (0)	3.28 (2996)	3.12 (63)
	cc-PVDZ	2.37 (677)	2.75 (1)	3.40 (3086)	3.27 (42)
Experimental (CH_3CN)[e]		2.14 (3.7)	2.52 (sh)	2.86 (4.3)	3.08 (sh)

[a] Molecule orientation as in Fig. 3.
[b] PM3 optimized geometry.
[c] HF/6-31G* optimized geometry.
[d] B3P86/6-31G* optimized geometry.
[e] Energies (eV) with parenthesized log ϵ values, Ref. 13e

description of the spectrum that was in a reasonable agreement with the experimental data even though this method does not include σ orbitals which, in analogy to the spectrum of neutral TTF, are expected to be involved in the lowest energy transitions. The extended Hückel method described the lowest energy absorption as a transition from the Semi-Occupied Molecular Orbital (SOMO) to the LUMO,[15] but this transition is expected to be polarized perpendicularly to the molecular plane of $TTF^{+\cdot}$, in sharp contradiction to the experimental data described above. Finally, the recent use of LNDO/S PERTCI[52] gives an accurate description of the two intense absorptions at 2.14 and 2.86 eV but does not account for the weak absorptions at 2.52 and 3.08 eV.

For the calculation of the absorption spectrum of $TTF^{+\cdot}$ we have used different theoretical methods ranging from semi-empirical to HF derived calculations and TD-DFT. As recently pointed out by Casida,[53] there are very few reports[54] in the literature on the application of TD-DFT to the study of the absorption spectra of open-shell species. Thus, TTF radical cations give us the chance to test the reliability of this method on sulfur containing radicals for the first time. The geometry of $TTF^{+\cdot}$ was optimized using PM3 for ZINDO calculations, HF/6-31G* for HF-based methods and B3P86/6-31G* for TD-DFT calculations and resulted in every case in a planar D_{2h} symmetry in agreement with other theoretical calculations[32b] and crystallographic data.[49] The assignment of the transitions was made relating the calculated oscillator strengths and polarizations to the experimental data and the results are gathered in Table 4.

It can be seen that TD-DFT calculations are clearly superior to the other used methods at calculating the excitation energies. Thus, three of the four calculated transitions are predicted with an accuracy of ca. 0.2 eV but the intense absorption at 2.86 eV is calculated with an error of 0.42–0.57 eV depending on the used basis set. It is well known that the accuracy of the TD-DFT procedure decreases with increase in the energy of the calculated transitions[11a,55] and it seems feasible that in this case, significant errors are found at energies above 2.5 eV. Concerning the basis set dependence of these calculations, the use of more flexible basis sets incorporating diffuse and polarization functions as well as triple split basis sets improves the calculation results but polarization functions play a more important role than diffuse ones probably due to the more compact excited state wave functions of cations compared to neutral molecules or anions.[54b] The B3P86/6-311G(2d,p) model chemistry yields the most accurate excitation energies of the used methods.

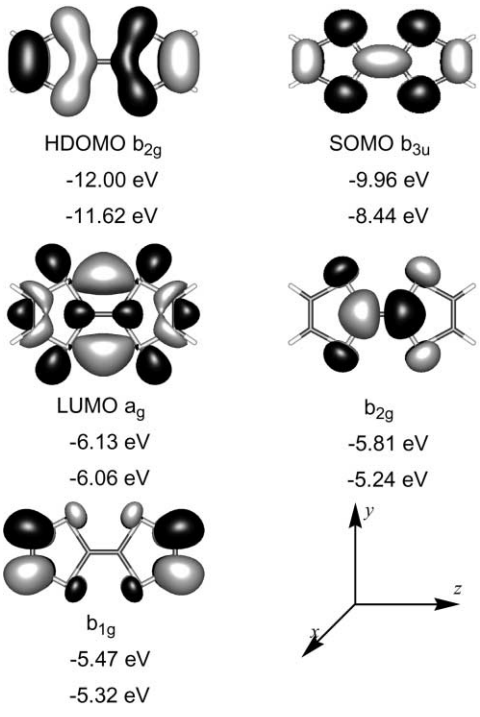

Figure 3. Molecular orbitals of $TTF^{+\cdot}$: UB3P86/6-31+G*//UB3P86/6-31G* (D_{2h}).

According to these calculations, the orbitals involved in the four lowest energy transitions are those depicted in Fig. 3.

The lowest energy absorption is due to a $b_{2g}\rightarrow b_{3u}$ transition from the Highest Doubly Occupied Molecular Orbital (HDOMO) to the SOMO that has B_{1u} symmetry and consequently is polarized in the long axis (z in Fig. 3) of the molecule. The absorption appearing as a shoulder at 2.52 eV is due to an $b_{3u}\rightarrow a_g$ (SOMO→LUMO) transition with B_{3u} symmetry and x polarization. The other two observed absorptions correspond to transitions from the SOMO to the two nearest unoccupied π orbitals: the most intense absorption located at 2.86 eV is a $b_{3u}\rightarrow b_{2g}$ transition with B_{1u} symmetry and z polarization, and the shoulder appearing at 3.08 eV is a $b_{3u}\rightarrow b_{1g}$ transition with B_{2u} symmetry and y polarization. These assignments are therefore in good agreement with the reported solution and polarized absorption spectra.

2.3.2. BEDT-TTF$^{+\cdot}$ and BEDO-TTF$^{+\cdot}$. Radical cations of TTF derivatives bearing chalcogen substituents give rise to an absorption band at ca. 1.2–1.3 eV in sharp contrast with other TTF derivatives whose radical cations display spectra analogous to that of unsubstituted TTF radical cation. This different behavior has given rise to two opposed interpretations. Thus, some authors[56,57] propose the formation of dimers on the basis of an analogous absorption observed[47c] in TTF_2^{2+} while others[13d,45,47b,50a,51] conclude that this is an intramolecular absorption since it is polarized in the long axis of the molecule, and moreover, intermolecular absorptions are observed at lower energies in these cases.

In an attempt to explain the large bathochromic shift observed in the lowest energy absorption of BEDO-TTF$^{+\cdot}$ and BEDT-TTF$^{+\cdot}$ with respect to TTF$^{+\cdot}$ we have studied the spectra of these radical cations. The geometry was optimized within the D_2 group of symmetry assuming the planarity of the TTF moiety predicted theoretically[32b] and found in crystal structures[58] of these radical ions. The UB3P86/6-31G* model chemistry was used in geometry optimizations and the calculations of excited states were performed using the less expensive 6-31G* basis set and the more accurate 6-311G(2d,p) basis set, while attempts to use the 6-31+G* basis set incorporating diffuse functions resulted in failures in the convergence of the TD-DFT procedure.

The results of these calculations are gathered in Table 5. In analogy to the above reported calculations on TTF$^{+\cdot}$, the first two lowest energy transitions are accurately calculated in every case. Above 2.5 eV the energies of the predicted absorptions clearly differ from the experimental ones to which they are assigned and the use of a more flexible basis set results only in a minor improvement of the calculated excitation energies.

In any case, these calculations allow an easy interpretation of the dramatic differences in the lowest energy absorption band of TTF$^{+\cdot}$ on the one hand and BEDT-TTF$^{+\cdot}$ and BEDO-TTF$^{+\cdot}$ on the other hand and discard the formation of dimers proposed by some authors to explain the spectrum of BEDT-TTF$^{+\cdot}$.[56] According to our calculations, the lowest energy band corresponds in every case to the transition of a β electron from the HDOMO to the SOMO, which is in good agreement with the observed polarization in the long axis of the molecule,[50] and the differences are only due to variations in the relative energy of these orbitals. Thus, the calculated energies using the UB3P86/6-31G* model chemistry in every case, are −11.56 eV for the β-HDOMO and −8.37 eV for the β-SOMO in TTF$^{+\cdot}$, −9.34 and −7.71 eV for BEDO-TTF$^{+\cdot}$ and −9.41 and −7.71 eV for BEDT-TTF$^{+\cdot}$, respectively. That means that the ethylenedioxy and ethylenedithio groups cause a destabilization of both the HDOMO and the SOMO but the energy of the former increases more than 2 eV while the latter increases only 0.66 eV causing an important decrease of the HDOMO–SOMO gap. The results of these calculations are in excellent agreement with the experimental gaps between the first and the second ionizations for TTF (1.88 eV), and BEDO-TTF (1.01 eV) determined by photoelectron spectroscopy.[59]

2.4. The UV–vis spectrum of TTF$^{2+\cdot}$

The UV–vis spectrum of TTF dication in acetonitrile has been reported[13c,e] to show intense absortions at 3.51 and 4.54 eV. And the only described theoretical calculations on this species used the PPP method to predict erroneously a bathochromic shift of the lowest energy absorption with respect to neutral TTF.[19]

The computational procedure we used was analogous to that described above for neutral molecules and radical ions. The geometry was first optimized using the B3P86/6-31G* model chemistry and a planar D_{2h} symmetry but the stationary point found in this way was characterized as a first order

Table 5. Calculated (TD-B3P86) and experimental energies (eV) with parenthesized oscillator strengths (10^4 f) for the lowest energy allowed transitions of radical cations of TTF derivatives

	BEDT-TTF$^{+\cdot}$(**3**$^{+\cdot}$)			BEDO-TTF$^{+\cdot}$(**4**$^{+\cdot}$)		
Transition[a]	6-31G*[b]	6-311G(2d,p)[b]	Exp.[c]	6-31G*[b]	6-311G(2d,p)[b]	Exp.[d]
B1	1.25 (1975)	1.24 (1816)	1.25	1.43 (1739)	1.42 (1513)	1.31
B3	2.24 (1)	2.16 (1)	2.07	2.15 (0)	2.08 (0)	2.06
B1	3.12 (1887)	2.98 (2401)	2.55	3.13 (2415)	2.99 (2299)	2.53
B2	2.59 (132)	2.88 (96)	2.71	2.90 (0)	2.84 (0)	2.69

[a] D_2 molecular symmetry with the z axis corresponding to the long molecular axis, y to the short molecular axis and x perpendicular to the main molecular plane.
[b] Molecular geometries optimized at B3P86/6-31G*.
[c] In CH_2Cl_2, Ref. 56.
[d] In CH_3OH, Ref. 13d.

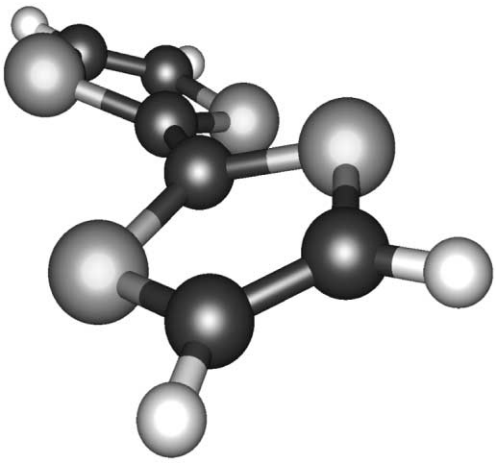

Figure 4. Optimized geometry of TTF^{2+}.

saddle point by the frequency analysis and therefore a geometry optimization without symmetry restrictions was performed. The minimum energy geometry presented D_2 symmetry with the two dithiole rings rotated one with respect to the other (Fig. 4) in analogy with the geometry calculated using a HF/6-31+G* model chemistry and the crystallographic structure of $TTF(ClO_4)_2$.[60]

In analogy with the calculations on radical cations (Section 2.3), we used the less expensive 6-31G* and the more accurate 6-311G(2d,p) basis sets, the latter affording slightly better excitation energies. Thus, a transition from the HOMO (MO51) to the LUMO (MO52) is responsible for the lowest energy absorption with a calculated energy of 3.42 eV and an oscillator strength of 0.3217. The second allowed transition is that from MO48 to MO52 with a calculated energy of 4.62 eV (4.65 eV using the 6-31G* basis set) and an oscillator strength of 0.051. The calculated energies match the experimental values with an error of 0.1 eV, showing an accuracy similar to that found in neutral TTF derivatives. For the sake of comparison, the calculated lowest excitation energy using other methods was 2.69 eV (CNDO/S//PM3), 2.66 eV (ZINDO//PM3) or 4.40 eV (CIS/6-31G*//HF/6-31G*).

2.5. NLO chromophores derived from TTF

Having established the reliability of TD-DFT calculations on a variety of simple TTF derivatives, we decided to study more complex TTF–π-acceptor chromophores, endowed with NLO properties.[9] The preparation of molecules containing a TTF derivative and a strong acceptor group revealed a very unusual[61] behavior in NLO active molecules: the energy of the lowest energy absorption increases on increasing the number of double bonds that link the donor and acceptor moieties. In order to clarify the effect that the number of double bonds plays, on the position of the lowest energy band, we have studied two series of compounds (Fig. 5). In the first series (compounds **5**[9b,62]) a TTF moiety is conjugated with a poor electron acceptor formyl group and these compounds display the normal bathochromic shift on increasing the number of double bonds. In the second one, compounds **6** containing a strong electron acceptor derived from thiobarbituric acid are studied as a model of the corresponding ethyl-substituted compounds (**7**) which show a hypsochromic shift on increasing the number of double bonds.[9c]

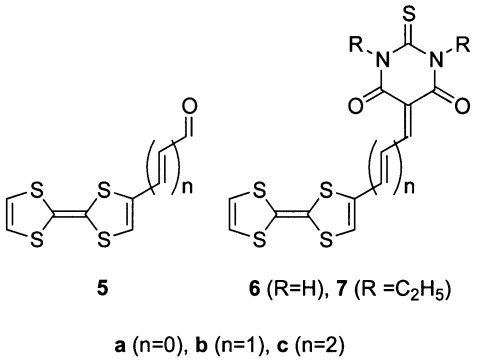

Figure 5. Structures of studied NLO phores.

Since our calculations using semiempirical (ZINDO, CNDO/S) and Hartree–Fock based methods (CIS) are completely unable to reproduce the spectra of these compounds (Table 6), we turned to TD-DFT calculations. The geometry of compounds **5** and **6** was optimized without symmetry restrictions and resulted in every case in a boat-like conformation of the TTF ring (Fig. 6) while the ethylenic spacer and the acceptor group lie in the same plane.

The calculated and experimental energies for the lowest lying transitions of compounds **5** and **6** are gathered in Table 6.

Table 6. Theoretical and experimental energy values (eV) with parenthesized oscillator strengths (10^4 *f*) for the lowest energy transitions (below 3.5 eV) of compounds **5** and **6**

	5a	5b	5c	6a		6b		6c	
Exp.	2.51[a]	2.41[a]	2.36[a]	1.73[b]	3.27[b]	1.88[b]	3.04[b]	1.92[b]	2.87[b]
ZINDO[c]	4.21 (1520)	3.95 (3860)	3.77 (8198)	3.27 (3536)	4.24 (3555)	3.20 (7610)	4.06 (3280)	3.13 (12821)	4.03 (2387)
CNDO/S[c]	4.76 (1833)	4.32 (5480)	3.99 (10793)	3.54 (5150)	5.08 (3128)	3.53 (9182)	4.49 (1785)	3.29 (13325)	4.43 (1620)
CIS[d]	4.41 (2698)	4.40 (5668)	4.24 (11681)	3.45 (5635)	5.14 (6605)	3.61 (12377)	4.70 (7433)	3.53 (21315)	4.51 (4162)
TD-B3P86[d]	2.25 (410)	2.13 (835)	1.99 (1313)	1.38 (1153)	3.24 (2375)	1.49 (1830)	3.04 (8588)	1.48 (2441)	2.85 (14603)

[a] In $CHCl_3$.
[b] Experimental values correspond to the analogous compound **7** in DMSO, Ref. 9c.
[c] PM3 optimized geometry.
[d] The calculations were performed using the 6-31+G* basis set on B3P86/6-31G* optimized geometries.

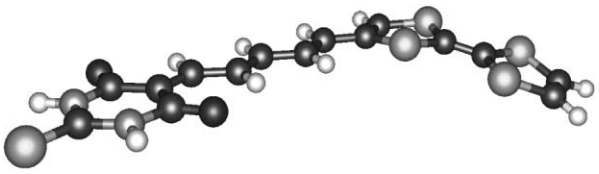

Figure 6. Optimized geometry of compound **6c**.

It can be seen that the TD-DFT calculated energies for the lowest energy absorptions are lower than the experimental values by 0.26–0.44 eV, which is an acceptable error for such large molecules that can be attributed to the poor prediction of charge-transfer transitions by DFT methods.[12a] Anyway, TD-DFT calculations clearly outperform semiempirical and CIS calculations that, for the same transitions, yield excitation energies that deviate from the experimental values by 1.21–2.25 eV. Furthermore, TD-DFT calculations provide a reasonable prediction of the experimental trends accounting for the bathochromic shift observed on passing from **5a** to **5b** and **5c**, the hypsochromic shift from **6a** to **6b** and the similar energies obtained for **6b** and **6c**.

The origin of the lowest energy absorption in compounds **5** and **6** is a charge transfer transition from the HOMO to the LUMO, with the former being analogous to the HOMO of unsubstituted TTF and the LUMO extending along the ethylenic spacer from the acceptor moiety to the first carbon atoms of the TTF ring (Fig. 7).

The changes in the energy of the CT transition are mainly due to changes in the HOMO–LUMO gap that decreases with increasing the number of double bonds in compounds **5** (**5a**: 2.81 eV, **5b**: 2.60 eV, **5c**: 2.38 eV), while remains nearly unaltered in compounds **6** (**6a**: 1.78 eV, **6b**: 1.72 eV, **6c**: 1.76 eV).

Furthermore, on going from **7a** to **7c** the second lowest energy absorption bands display a bathochromic shift (3.27 eV for **7a**, 3.04 eV for **7b** and 2.87 eV for **7c**), the energies of these transitions being accurately predicted by our calculations (**6a**: 3.24 eV; **6b**: 3.04 eV; **6c**: 2.85 eV), maybe due to their lack of charge-transfer character.

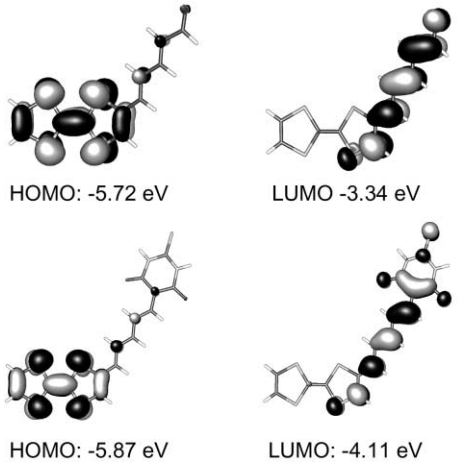

Figure 7. HOMO and LUMO of compounds **5c** (top) and **6c** (bottom): B3P86/6-31+G*//B3P86/6-31G*.

Thus, TD-DFT calculations account for the different bathochromic and hypsochromic shifts observed in these TTF-based chromophores, allowing a rationalization of their optical properties.

3. Conclusions

The TD-DFT approach has been applied to the study of the UV–vis spectra of TTF derivatives for the first time. This method provides excitation energies with high accuracy compared to semiempirical (CNDO/S, ZINDO) and ab initio methods, such as CIS or TD-HF, which involve a comparable computational cost. Furthermore, the minimal basis set dependence makes the method suitable for large molecules for which large basis sets should result in extremely large resource requirements. The calculated transition energies, as well as the oscillator strengths and polarizations are in very good agreement with the reported absorption spectra.

TD-DFT calculations have also been applied to the study of the optical properties of TTF-derived radical cations, which are the first sulfur-containing open-shell species to be studied by this method. While low excitation energies are accurately predicted, the performance of the TD-DFT method is poorer at higher energies. The effect of chalcogen substituents (O, S) at the periphery of the TTF, which results in a large bathochromic shift of the lowest energy absorption bands of $\mathbf{3}^{+\cdot}$ and $\mathbf{4}^{+\cdot}$ compared to $\mathbf{1}^{+\cdot}$, is precisely reproduced. This is a consequence of the decreased HDOMO–SOMO gap in $\mathbf{3}^{+\cdot}$ and $\mathbf{4}^{+\cdot}$, thus confirming the intramolecular nature of this absorption.

The excitation energies of charge-transfer transitions in TTF-derived chromophores for nonlinear optics are also predicted with reasonable accuracy and calculations account for the surprising hypsochromic shift of the charge-transfer absorption observed in some of these chromophores on extending the conjugation path.

To sum up, TD-DFT appears as a valuable general method in the calculation of the excitation energies of TTF derivatives, both in their neutral and oxidized (radical cations and dications) states. These calculations can be a valuable help in the interpretation of spectroelectrochemical experiments and in the design of new chromophores incorporating TTF moieties.

4. Computational procedure

All the calculations were performed with the GAUSSIAN 98[63] program with the only exception of the CNDO/S calculations that used the MOS-F[64] program.

The Berny analytical gradient method was used for geometry optimizations with the default threshold values for the maximum force and displacement. Stationary points were characterized as minima by the absence of imaginary frequencies. Excited state calculations using CIS or TD were solved for a minimum of six states using the *nstates* option of the CIS and TD keywords. Processing of the

results of molecular orbital calculations was achieved with the MOLDEN-3.6 program.[65]

Acknowledgements

We are grateful to Dr Belén Villacampa for the recording of the UV–vis spectra of compounds **4**, **5** and **7**. We thank DGICYT (Project MAT99-1009-C02-02) for financial support.

Addendum. After submission of this manuscript a paper by J. Fabian dealing with TD-DFT calculations on sulfur compounds including TTF and $TTF^{+\cdot}$ has been published on the web: Fabian, J. *Theor. Chem. Acc.* **2001**, DOI 10.1007/s002140100250. We thank Professor J. Fabian for bringing this paper to our attention.

References

1. (a) Garín, J. *Adv. Heterocycl. Chem.* **1995**, *62*, 249–304. (b) Schukat, G.; Fanghänel, E. *Sulfur Rep.* **1996**, *18*, 1–294.
2. Williams, J. M.; Ferraro, F. R.; Thorn, J. R.; Carlson, K. D.; Geiser, U.; Wang, H. H.; Kini, A. M.; Whangbo, M.-H. *Organic Superconductors (Including Fullerenes)*; Prentice Hall: Englewood Cliffs, NJ, 1992.
3. Le Derf, F.; Mazari, M.; Mercier, N.; Levillain, E.; Richomme, P.; Becher, J.; Garín, J.; Orduna, J.; Gorgues, A.; Sallé, M. *Inorg. Chem.* **1999**, *38*, 6096–6100.
4. Nakamura, T. In *Handbook of Organic Conductive Molecules and Polymers*; Nalwa, H. S., Ed.; Wiley: New York, 1997; pp 727–780.
5. (a) Jørgensen, T.; Hansen, T. K.; Becher, J. *Chem. Soc. Rev.* **1994**, *23*, 4151. (b) Nielsen, M. B.; Lomholt, C.; Becher, J. *Chem. Soc. Rev.* **2000**, *29*, 153–164.
6. (a) Bryce, M. R. *Adv. Mater.* **1999**, *11*, 11–23. (b) Bryce, M. R. *J. Mater. Chem.* **2000**, *10*, 589–598.
7. (a) Guldi, D. M.; González, S.; Martín, N.; Antón, A.; Garín, J.; Orduna, J. *J. Org. Chem.* **2000**, *65*, 1978–1983. (b) Martín, N.; Sánchez, L.; Herranz, M. A.; Guldi, D. M. *J. Phys. Chem. A* **2000**, *104*, 4648–4657. (c) Martín, N.; Sánchez, L.; Guldi, D. M. *Chem. Commun.* **2000**, 113–114.
8. (a) Martín, N.; Sánchez, L.; Illescas, B.; Pérez, I. *Chem. Rev.* **1998**, *98*, 2527–2547. (b) Guldi, D. M. *Chem. Commun.* **2000**, 321–327.
9. (a) de Lucas, A. I.; Martín, N.; Sánchez, L.; Seoane, C.; Andreu, R.; Garín, J.; Orduna, J.; Alcalá, R.; Villacampa, B. *Tetrahedron* **1998**, *54*, 4655–4662. (b) González, M.; Martín, N.; Segura, J. L.; Garín, J.; Orduna, J. *Tetrahedron Lett.* **1998**, *39*, 3269–3272. (c) Garín, J.; Orduna, J.; Rupérez, J. I.; Alcalá, R.; Villacampa, B.; Sánchez, C.; Martín, N.; Segura, J. L.; González, M. *Tetrahedron Lett.* **1998**, *39*, 3577–3580. (d) Herranz, M. A.; Martín, N.; Sánchez, L.; Garín, J.; Orduna, J.; Alcalá, R.; Villacampa, B.; Sánchez, C. *Tetrahedron* **1998**, *54*, 11651–11658. (e) González, M.; Martín, N.; Segura, J. L.; Seoane, C.; Garín, J.; Orduna, J.; Alcalá, R.; Sánchez, C.; Villacampa, B. *Tetrahedron Lett.* **1999**, *40*, 8599–8602.
10. (a) Wolff, J. J.; Wortmann, R. *Adv. Phys. Org. Chem.* **1999**, *32*, 121–217. (b) Zyss, J.; Ledoux, I.; Nicoud, J.-F. In *Molecular Nonlinear Optics. Materials, Physics, and Devices*; Zyss, J., Ed.; Academic: London, 1994; pp 129–200.
11. (a) Stratmann, R. E.; Scuseria, G. E.; Frisch, M. J. *J. Chem. Phys.* **1998**, *109*, 8218–8224. (b) Koch, W.; Holthausen, M. C. *A Chemist's Guide to Density Functional Theory*; Wiley–VCH: Weinheim, 2000.
12. (a) Tozer, D. J.; Amos, R. D.; Handy, N. C.; Roos, B. O.; Serrano-Andrés, L. *Mol. Phys.* **1999**, *97*, 859–868. (b) Petiau, M.; Fabian, J.; Rosmus, P. *Phys. Chem. Chem. Phys.* **1999**, *1*, 5547–5554. (c) Fabian, J.; Mann, M.; Petiau, M. *J. Mol. Model.* **2000**, *6*, 177–185. (d) Moreno-Mañas, M.; Pleixats, R.; Andreu, R.; Garín, J.; Orduna, J.; Villacampa, B.; Levillain, E.; Sallé, M. *J. Mater. Chem.* **2001**, *11*, 374–380. (e) Petiau, M.; Fabian, J. *J. Mol. Struct. (Theochem)* **2001**, *538*, 253–260.
13. (a) Klots, C. E.; Compton, R. N.; Raaen, V. F. *J. Chem. Phys.* **1974**, *60*, 1177–1178. (b) Sandman, D. J.; Holmes, T. J.; Warner, D. E. *J. Org. Chem.* **1979**, *44*, 880–882. (c) Schukat, G.; Fanghänel, E. *J. Prakt. Chem.* **1985**, *327*, 767–774. (d) Senga, T.; Kamoshida, K.; Kushch, L. A.; Saito, G.; Inayoshi, T.; Ono, I. *Mol. Cryst. Liq. Cryst.* **1997**, *296*, 97–143. (e) Hünig, S.; Kiesslich, G.; Quast, H.; Scheutzow, D. *Liebigs Ann. Chem.* **1973**, 310–323. (f) Wudl, F.; Smith, G. M.; Hufnagel, E. J. *J. Chem. Soc., Chem. Commun.* **1970**, 1453–1454.
14. (a) Engler, E. M.; Scott, B. A.; Etemad, S.; Penney, T.; Patel, V. V. *J. Am. Chem. Soc.* **1977**, *99*, 5909–5916. (b) Wudl, F.; Kruger, A. A.; Kaplan, M. L.; Hutton, R. S. *J. Org. Chem.* **1977**, *42*, 768–770.
15. Coffen, D. L.; Chambers, J. Q.; Williams, D. R.; Garrett, P. E.; Canfield, N. D. *J. Am. Chem. Soc.* **1971**, *93*, 2258–2268.
16. Gleiter, R.; Schmidt, E.; Cowan, D. O.; Ferraris, J. P. *J. Electron Spectorsc.* **1973**, *2*, 207–210.
17. Bennett, B. I.; Herman, F. *Chem. Phys. Lett.* **1975**, *32*, 334–337.
18. Trsic, M.; Laidlaw, W. G. *Int. J. Quantum Chem.* **1982**, *21*, 557–563.
19. Zaradnik, R.; Carsky, P.; Hünig, S.; Kiesslich, G.; Scheutzow, D. *Int J. Sulfur Chem.* **1971**, *C6*, 109–122.
20. Gleiter, R.; Kobayashi, M.; Spanget-Larsen, J.; Ferraris, J. P.; Bloch, A. N.; Bechgaard, K.; Cowan, D. O. *Ber. Bunsenges. Physik. Chem.* **1975**, *79*, 1218–1226.
21. Batsanov, A. S.; Bryce, M. R.; Heaton, J. N.; Moore, A. J.; Skabara, P. J.; Howard, J. A. K.; Ortí, E.; Viruela, P. M.; Viruela, R. *J. Mater. Chem.* **1995**, *5*, 1689–1696.
22. Stewart, J. J. P. *J. Comput. Chem.* **1989**, *10*, 20–220.
23. (a) Del Bene, J.; Jaffé, H. H. *J. Chem. Phys.* **1968**, *48*, 1807–1813. (b) Del Bene, J.; Jaffé, H. H. *J. Chem. Phys.* **1968**, *48*, 4050–4055.
24. Zerner, M. C. *Reviews in Computational Chemistry*; Lipkowitz, K. B., Boyd, D. B., Eds.; VCH: New York, 1991; Vol. 2, pp 313–365.
25. Foresman, J. B.; Head-Gordon, M.; Pople, J. A.; Frisch, M. J. *J. Phys. Chem.* **1992**, *96*, 135–149.
26. Dunning, T. H.; McKoy, V. *J. Chem. Phys.* **1967**, *47*, 1735–1747.
27. (a) Bauernschmitt, R.; Ahlrichs, R. *Chem. Phys. Lett.* **1996**, *256*, 454–464. (b) Adamo, C.; Scuseria, G. E.; Barone, V. *J. Chem. Phys.* **1999**, *111*, 2889–2899.
28. Becke, A. D. *J. Chem. Phys.* **1993**, *98*, 5648–5652.
29. The B3P86 functional consists of Becke's three parameter hybrid functional[28] with the nonlocal correlation provided by the Perdew 86 expresion: Perdew, J. P. *Phys. Rev. B* **1986**, *33*, 8822–8824.
30. The B3PW91 Functional consists of Becke's three parameter hybrid functional[28] with the nonlocal correlation provided by

the Perdew 91 expression: Perdew, J. P.; Burke, K.; Wang, Y. *Phys Rev. B* **1996**, *54*, 16533–16539.
31. Wiberg, K. B.; Stratmann, R. E.; Frisch, M. J. *Chem. Phys. Lett.* **1998**, *297*, 60–64.
32. (a) Viruela, R.; Viruela, P. M.; Pou-Amérigo, R.; Ortí, E. *Synth. Met.* **1999**, *103*, 1991–1992. (b) Demiralp, E.; Goddard III, W. A. *J. Phys. Chem. A* **1997**, *101*, 8128–8131.
33. Liu, R.; Zhou, X.; Kasmai, H. *Spectrochim. Acta A* **1997**, *53*, 1241–1256.
34. Ma, B.; Lii, J.-H.; Schaefer III, H. F.; Allinger, N. L. *J. Phys. Chem.* **1996**, *100*, 8763–8769.
35. Altmann, J. A.; Handy, N. C.; Ingamells, V. E. *Mol. Phys.* **1997**, *92*, 339–352.
36. Terkia-Derdra, N.; Andreu, R.; Sallé, M.; Levillain, E.; Orduna, J.; Garín, J.; Ortí, E.; Viruela, R.; Pou-Amerigo, R.; Sahraoui, B.; Gorgues, A.; Favard, J.-F.; Riou, A. *Chem. Eur. J.* **2000**, *6*, 1199–1213.
37. Hargittai, I.; Brunvoll, J.; Kolonits, M.; Khodorkovsky, V. *J. Mol. Struct.* **1994**, *317*, 273–277.
38. Hariharan, P. C.; Pople, J. A. *Theor. Chim. Acta* **1973**, *28*, 213–222.
39. Krishnan, R.; Binkley, J. S.; Seeger, R.; Pople, J. A. *J. Chem. Phys.* **1980**, *72*, 650–654.
40. (a) Woon, D. E.; Dunning, Jr., T. H. *J. Chem. Phys.* **1993**, *98*, 1358–1371. (b) Kendall, R. A.; Dunning Jr, T. H.; Harrison, R. J. *J. Chem. Phys.* **1992**, *96*, 6796–6806.
41. (a) Demilralp, E.; Dasgupta, S.; Goddard III, W. A. *J. Am. Chem. Soc.* **1995**, *117*, 8154–8158. (b) Demilralp, E.; Dasgupta, S.; Goddard III, W. A. *J. Phys. Chem. A* **1997**, *101*, 1975–1981.
42. Guioneau, P.; Chasseau, D.; Howard, J. A. K.; Day, P. *Acta Crystallogr.* **2000**, *C56*, 453–454.
43. Suzuki, T.; Yamochi, H.; Srdanov, G.; Hinkelmann, K.; Wudl, F. *J. Am. Chem. Soc.* **1989**, *111*, 3108–3109.
44. Gol'denberg, L. M.; Aldoshina, M. Z.; Lyubovskaya, R. N.; Chibisova, T. A.; Rodionov, V. Ya.; Khodorkovskii, V. Yu.; Neiland, O. Ya. *Bull. Acad. Sci. USSR* **1985**, *34*, 1934–1936.
45. Horiuchi, S.; Yamochi, H.; Saito, G.; Sakaguchi, K.; Kusunoki, M. *J. Am. Chem. Soc.* **1996**, *118*, 8604–8622.
46. This shoulder is discernible in Fig. 5 of Ref. 45, although it is not alluded to in the text.
47. (a) Huchet, L.; Akoudad, S.; Levillain, E.; Roncali, J.; Emge, A.; Bauerle, P. *J. Phys. Chem. B* **1998**, *102*, 7776–7781. (b) Zimmer, K.; Godicke, B.; Hoppmeier, M.; Meyer, H.; Schweig, A. *Chem. Phys.* **1999**, *248*, 263–271. (c) Torrance, J. B.; Scott, B. A.; Welber, B.; Kaufman, K. B.; Seiden, P. E. *Phys. Rev. B* **1979**, *19*, 730–741.
48. Sugano, T.; Yakushi, K.; Kuroda, H. *Bull. Chem. Soc. Jpn* **1978**, *51*, 1041–1046.
49. Yakushi, K.; Nishimura, S.; Sugano, T.; Kuroda, H.; Ikemoto, I. *Acta Crystallogr.* **1980**, *B36*, 358–363.
50. (a) Sugano, T.; Hayashi, H.; Kinoshita, M.; Nishikida, K. *Phys. Rev. B* **1989**, *39*, 11387–11397. (b) Sugano, T.; Hayashi, H.; Takenouchi, H.; Nishikida, K.; Urayama, H.; Yamochi, H.; Saito, G.; Kinoshita, M. *Phys. Rev. B* **1988**, *37*, 9100–9102.
51. Yoshitake, M.; Yakushi, K.; Kuroda, H.; Kobayashi, A.; Kato, R.; Kobayashi, H. *Bull. Chem. Soc. Jpn* **1988**, *61*, 1115–1119.
52. Zimmer, K.; Gödicke, B.; Hoppmeier, M.; Meyer, H.; Schweig, A. *Chem. Phys.* **1999**, *248*, 263–271.
53. Guan, J.; Casida, M. E.; Salahub, D. R. *J. Mol. Struct. (Theochem)* **2000**, *527*, 229–244.
54. (a) Hirata, S.; Head-Gordon, M. *Chem. Phys. Lett.* **1999**, *302*, 375–382. (b) Hirata, S.; Lee, T. J.; Head-Gordon, M. *J. Chem. Phys.* **1999**, *111*, 8904–8912. (c) Halasinski, T. M.; Hudgins, D. M.; Salama, F.; Allamandola, L. J.; Bally, T. *J. Phys. Chem. A* **2000**, *104*, 7484–7491.
55. Casida, M. E.; Jamorski, C.; Casida, K. C.; Salahub, D. R. *J. Chem. Phys.* **1998**, *108*, 4439–4449.
56. (a) Kozlov, M. E.; Tanaka, Y.; Tokumoto, M.; Tani, T. *Chem. Phys. Lett.* **1994**, *223*, 318–322. (b) Kozlov, M. E.; Tanaka, Y.; Tokumoto, M.; Tani, T. *Synth. Met.* **1995**, *70*, 987–988.
57. Spanggaard, H.; Prehn, J.; Nielsen, M. B.; Levillain, E.; Allain, M.; Becher, J. *J. Am. Chem. Soc.* **2000**, *122*, 9486–9494.
58. (a) Abboud, K. A.; Chou, L.-K.; Clevenger, M. B.; De Oliveira, G. F.; Talham, D. R. *Acta Crystallogr.* **1995**, *C51*, 2356–2362. (b) Liu, H.-L.; Chou, L.-K.; Abboud, K. A.; Ward, B. H.; Fanucci, G. E.; Granroth, G. E.; Canadell, E.; Meisel, M. W.; Talham, D. R.; Tanner, D. B. *Chem. Mater.* **1997**, *9*, 1865–1877. (c) Bu, X.; Cisarova, I.; Coppens, P. *Acta Crystallogr.* **1992**, *C48*, 1558–1560.
59. Lichtenberger, D. L.; Johnston, R. L.; Hinkelmann, K.; Suzuki, T.; Wudl, F. *J. Am. Chem. Soc.* **1990**, *112*, 3302–3307.
60. (a) Ashton, P. R.; Balzani, V.; Becher, J.; Credi, A.; Fyfe, M. C. T.; Mattersteig, G.; Menzer, S.; Nielsen, M. B.; Raymo, F. M.; Stoddart, J. F.; Venturi, M.; Williams, D. J. *J. Am Chem. Soc.* **1999**, *121*, 3951–3957. (b) Although the full structures of TTF Cl_2 and TTF Br_2 were never reported, the torsion angle between the two dithiole rings of TTF^{2+}(ca. 60°) was first reported in: Scott, B. A.; La Placa, S. J.; Torrance, J. B.; Silvermann, B. D.; Welber, B. *J. Am. Chem. Soc.* **1977**, *99*, 6631–6639.
61. (a) A hypsochromic effect on extension of conjucation has recently been noted in some push–pull stilbenoid chromophores: Meier, H.; Petermann, R.; Gerold, J. *Chem. Commun.* **1999**, 977–978. (b) A similar phenomenon has been observed for vinylogous indigo dyes: Fabian, J.; Hartmann, H. *Light Absorption of Organic Colorants*; Springer: Berlin, 1980.
62. Garín, J.; Orduna, J.; Uriel, S.; Moore, A. J.; Bryce, M. R.; Wegener, S. W.; Yufit, D. S.; Howard, J. A. K. *Synthesis* **1994**, 489–493.
63. Frisch, M. J.; Trucks, G. W.; Schlegel, H. B.; Scuseria, G. E.; Robb, M. A.; Cheeseman, J. R.; Zakrzewski, V. G.; Montgomery, J. A.; Stratmann, R. E.; Burant, J. C.; Dapprich, S.; Millan, J. M.; Daniels, A. D.; Kudin, K. N.; Strain, M. C.; Farkas, O.; Tomasi, J.; Barone, V.; Cossi, M.; Cammi, R.; Mennucci, B.; Pomelli, C.; Adamo, C.; Clifford, S.; Ochterski, J.; Pettersson, G. A.; Ayala, P. Y.; Cui, Q.; Morokuma, K.; Malick, D. K.; Rabuck, A. D.; Raghavachari, K.; Foresman, J. B.; Cioslowski, J.; Ortiz, J. V.; Baboul, A. G.; Stefanov, B. B.; Liu, G.; Liashenko, A.; Piskorz, P.; Komaromi, I.; Gomperts, R.; Martin, R. L.; Fox, D. J.; Keith, T.; Al-Laham, M. A.; Peng, C. Y.; Nanayakkara, A.; Challacombe, M.; Gill, P. M. W.; Johnson, B.; Chen, W.; Wong, M. W.; Andres, J. L.; González, C.; Head-Gordon, M.; Replogle, E. S.; Pople, J. A. GAUSSIAN 98, Revision A.9; Gaussian, Inc: Pittsburgh, PA, 1998.
64. MOS-F V4 (Fujitsu Ltd, 1998).
65. Schaftenaar, G.; Noordik, J. H. *J. Comput.-Aided Mol. Design* **2000**, *14*, 123–134.